Normal and skew multipole terms in the dipoles and quadrupoles of the 12 GeV CEBAF upgrade.

Yves Roblin

JLAB-TN-08-042

Abstract

This paper gives an estimate of the maximum acceptable level for the multipole components of the dipole and quadrupoles in the 12 GeV upgrade. Previous work yielded the specifications for the normal multipoles for dipoles and quadrupoles in Arc 10. This work extends the specification to all the dipoles and quadrupoles in the machine and also sets limits on the skew components.

It is found that the skew quadrupole term has to be kept at or below 1 Gauss/cm in order to meet the specifications. Higher order skew terms can be specified together with the normal term in terms of the resulting amplitude. For this reason, the original specification on the amplitude of the normal multipole terms was recast to specify the total amplitude including the skew terms contribution. The final specification was tracked through the machine and validated in terms of its effect on the phase-space and halo.

1 introduction

The 12GeV CEBAF upgrade will require a tenth arc. Synchrotron radiation effects will produce a significantly larger beam than in the original 6 GeV machine. As a consequence, the sensitivity to field inhomogeneities is greater. Field inhomogeneities arise as a result of machine and assembly errors, steel saturation and imperfect pole shapes.

Excessive multipole content affect steering and also increases emittance growth. A specification that restricts the amount of emittance growth is given for both normal and skew multipoles. We followed an approach analogous to the one adopted the original work [1] and adapt it for the inclusion of skew multipoles.

2 definitions

2.1 normal and skew multipoles

Magnetic fields are derived from a potential function which is the solution to the Laplace equations. In general, this potential is expressed as a Taylor expansion

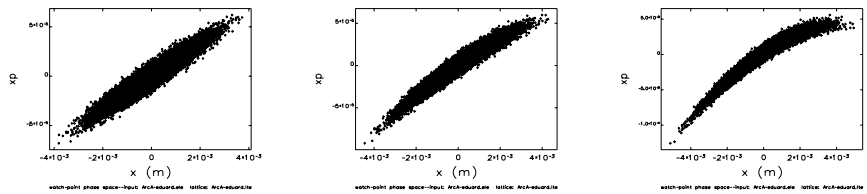

Figure 1: xx' phase space distribution at end of ArcA for 0, 0.5 and 1.0 m^{-3} normal sextupole strengths

in the complex plane.

The magnetic field can be obtained by differentiation of the complex potential which has both an imaginary part and a real part. The imaginary part represents the midplane symmetry solution and the coefficients of the expansion are *normal multipoles*.

The real solution is the part corresponding to the out-of-plane situation (rotated magnet) where one has coupling between the transverse dimensions. The expansion exhibits the *skew multipoles*.

Each multipole component contributes to the integrated field according to the polynomial expansion (in DIMAD utransport conventions)

$$B(x)L = (B\rho)\sum_n K_n L x^n \tag{1}$$

2.2 good field region

The 12GeV field specifications are defined relative to the design orbit. Due to steering offsets, pathlength errors, optics measurements allowance and so on, the actual orbit will be deviating from this design orbit. Hence, one requires the field to satisfy the specifications in the cross-sectional area bounded by

$$|x, y| < S + m + 4\sigma(x, y)$$

where S is the steering allowance of 1mm, m is the optics measurement allowance of 2mm and sigma the beam size.

3 cross-comparison with DIMAD calculations

The beam was tracked through the Arc and the second-moments of the particle distribution were computed at the end of the line. From these, the β_m, α_m and ϵ_m of the new mismatched distribution were obtained. Typical phase-space distributions are shown in figure1

Each multipole was varied individually covering a range of effects from small distortion of the phase space to large tails and particle loss. That procedure was repeated for twenty random orbits distributed uniformly within the good

field region. The amount of mismatch was evaluated for each dataset for the X and Y planes independently.

3.1 generation of multipole content

Systematic and random multipoles were studied in the dipoles. The former were distributed uniformly along the lattice, giving the same value for all dipoles in the arc. We repeated the simulation for positive and negative values.

The random multipoles were allowed to vary between $-K_nL$ and $+K_nL$ for each dipole. The sampling was repeated twenty times for each orbit.

3.1.1 test orbits

The test orbits were generated by randomly offsetting the beam at the entrance of the Arc in order to probe the totality of the good field region. Figure 2 shows the coverage.

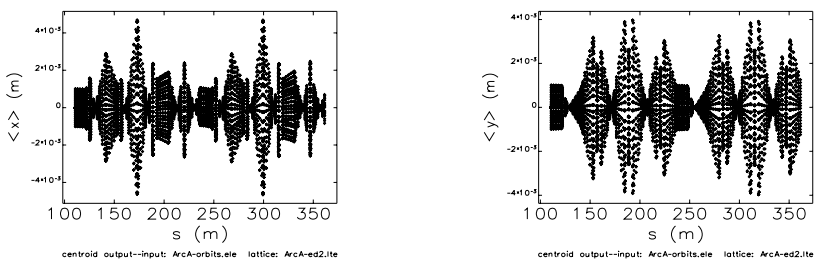

Figure 2: Coverage of the test orbits

3.2 measure of the beam mismatch

As a measure of the mismatch, we use the ratio of the emittances between the matched design ellipse and the emittance of the design ellipse that would be needed to encompass the mismatched ellipse arising from multipoles. This is the same definition that was employed in [1].

Figure 3 shows the original matched ellipse (red), along with the mismatched ellipse resulting from multipole components (green) and the final re-matched ellipse for which the twiss parameters of the beam are adapted to the transport parameters at the entrance of the next linac.

The ratio between the areas of this ellipse and the original matched ellipse is the measure of mismatch. It is possible to compute this ratio analytically. The easiest way to do so is to transform the mismatched beam into the Floquet frame of the design beam. In this frame, rematching is a simple matter of increasing the radius of the design circle until it encompasses the mismatched ellipse.

In [1], this procedure was carried out by hand in a Matlab program.

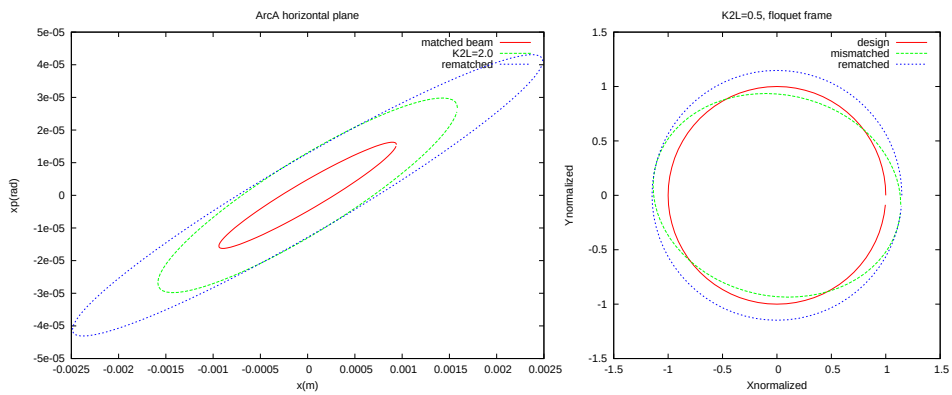

Figure 3: beam ellipses after tracking through ArcA with a sextupole component

We fitted $\beta_{x0}(\beta_x)$,$\alpha_{x0}(\alpha_x)$,$\gamma_{x0}(\gamma_x)$,$\epsilon_{x0}(\epsilon_x)$ the twiss parameters for the original and mismatched ellipse respectively by transporting a particle bunch through ArcA. Care was taken to use enough particles (10000) to produce reliable fits for the twiss parameters.

The mismatched parameters can then be transformed into the Floquet frame with

$$\beta_{xf} = \frac{\beta_x}{\beta_{x0}} \tag{2}$$

$$\gamma_{xf} = \frac{\alpha_{x0}}{\beta_{x0}}\beta_x - 2\alpha_x\alpha_{x0} + \beta_{x0}\gamma_x \tag{3}$$

It can be shown that the transport matrix eigenvectors are the major and minos axises of this phase space ellipse. Rematching in the Floquet frame consist in encompassing the ellipse by a circle whose radius is equal to the major axis of that mismatched ellipse.

The eigenvalue giving the length of the major axis is

$$h = \frac{1}{2}\left(\gamma_{xf} + \beta_{xf}\right) \tag{4}$$

$$a = \sqrt{h+1} + \sqrt{h-1} \tag{5}$$

which finally yields the area E (emittance) of the rematched circle and consequently, the mismatch M defined as the ratio between that area and the mismatched ellipse area (emittance).

$$E = \frac{a^2}{2}\epsilon_x \tag{6}$$

$$M = \frac{E}{\epsilon_0} - 1 \tag{7}$$

We checked that our analytical approach gave the same results as the manual Matlab procedure carried out in [1].

3.3 Linear errors

We first investigated the effect of normal quadrupole errors in the dipoles (the so-called body gradient). A quadrupole gradient can arise during the fabrication and assembly of dipole magnets if the pole faces are not perfectly parallel. It is reasonable to assume that this is a systematic error, identical for all the dipoles of the same type since they were all machined following the same process, by the same manufacturer.

An earlier note gives magnetic measurements made on the 1 meter magnet[10] where the value was estimated to be $\frac{B^{'}L}{BL} = 0.03m^{-1}$.

More recent beam based measurements [3] are listed in table 1.

Magnet Type	$\frac{B'L}{BL}m^{-1}$
BE 1 meter	0.0233
BB 2 meters	0.0192
BA 3 meters	0.00712

Table 1: July 2004 Beam based measurement of body gradients.

In order to set an upper limit on the amount of normal quadrupole component that can be tolerated, we carried out a set of simulations where the body gradient was gradually increased and the fodo structure of the Arc restored by adjusting the Arc quadrupoles accordingly. We were able to go as high as $K_1 = 0.002m^{-2}$.

Given that

$$\begin{aligned} \frac{B'L}{BL} &= \frac{B'L}{B\rho}\frac{\rho}{L} \\ &= K_1 L \frac{\rho}{L} \\ &= \frac{K_1 L}{\theta} \end{aligned}$$

We get an upper limit for the maximum allowed normal quadrupole error of $\frac{B'L}{BL} \leq 0.8m^{-1}$. This is many times above what we actually observe in the existing dipoles.

3.4 normal sextupole random errors

Table 2 shows the amount of mismatch in percent relative to the amplitude of the random sextupole component. The error bar represents the range of values that were present. This data is generated from twenty orbits, with twenty random datasets per orbit.

If one wishes to always remain under 10 percent of mismatch, a value of $K_2L < 0.4$ is adequate.

We repeated the study for the octupole term (K_4L) and again, found results compatible with the earlier study.

K2L (m^{-2})	Mx	My	M
0.05	4.1 ± 1.3	3.0 ± 0.6	4.3
0.1	5.1 ± 1.6	2.7 ± 0.9	5.7
0.15	4.7 ± 1.6	3.5 ± 1.2	5.8
0.2	5.9 ± 2.0	4.9 ± 1.6	7.6
0.3	6.7 ± 2.2	5.3 ± 1.8	8.5
0.4	12.6 ± 4.5	6.2 ± 2.2	14.0
0.5	13.7 ± 5.0	5.2 ± 2.0	14.6
1.0	15.3 ± 5.5	14.8 ± 5.3	21.2

Table 2: Mismatch in percent for each plane for increasing values of sextupole component.Proposed specification is above the horizontal line

4 Estimating higher order terms for quadrupoles

Quadrupole errors can be partitioned in systematic (pole shape, saturation) and random (contruction) errors.

In [7], measurements done upon receipt of the QA quadrupole during the construction phase of CEBAF were recently reexamined. This data set consisted of 126 measurements on 103 magnets. The normal component for all the multipoles up to n=20 were measured initially over a current range from 1 to 10 Amps. The particle tracking program ELEGANT [2], allows for the inclusion of both systematic and random, normal and skew components for quadrupoles. A utility *sddsrandmult* is provided in this sofware package which implements the formalism presented in [9] by Halbach. This parametrization is well known and commonly used for estimated construction errors on magnets. This utility was used to reproduce the multipole distribution found in the measurements by varying the construction errors until they reproduced the measured spectrum.

Multipole term	$\frac{DB}{B}$ rand.	$\frac{DB}{B}$ syst.	$\frac{DB}{B}$ poz.
n=2	2.6e-3	0.0	0.0
n=3	4.6e-3	0.0	3e-3
n=4	1.8e-3	0.0	0.0
n=5	2.2e-3	9e-4	5e-3
n=6	3.0e-3	0.0	0.0
n=7	4.6e-3	0.0	0.0
n=8	5e-3	0.0	0.0
n=9	5e-3	2e-3	5e-3

Table 3: Proposed quadrupole specifications at the pole tip and comparison with previous one.

It turns out that this required an error of about 1/5 of the allowed errors specified by the technical drawings.

In order to estimate the systematic errors, the author of [7] postulated that since the saturation effects are small at the pole tips (they are mainly located at

the root of the steel by design), the systematics errors are due to the geometry of the pole shape and will appear in the allowed multipole terms on top of the construction errors. By comparing the allowed multipole sigma/mean with the unallowed multipoles, the systematics where attributed to the widening of the spectrum for the allowed terms. Assuming further that they added in quadrature with the random errors yielded the estimate.

Values proposed in [7] for simulated real quadrupoles as measured are summarized in table 3 in terms of errors normalized to the quadrupole field B at the tip. Similarly to what we did for the dipoles, we multipled the original values by a factor of five to set the actual specification. A full-tracking was then performed with all dipoles and quadrupole specifications to check for validity.

Another cross-comparison that can be made is with earlier tracking results. The first two columns show the random and systematics field errors we proposed for the upper bound in this specification. In the third column labeled $\frac{\Delta B}{B}_{poz}$, the numbers obtained for Arc10 in [1] are shown.

This new proposed specification is in line with those earlier results.

4.1 Comparison with new MQA measurement

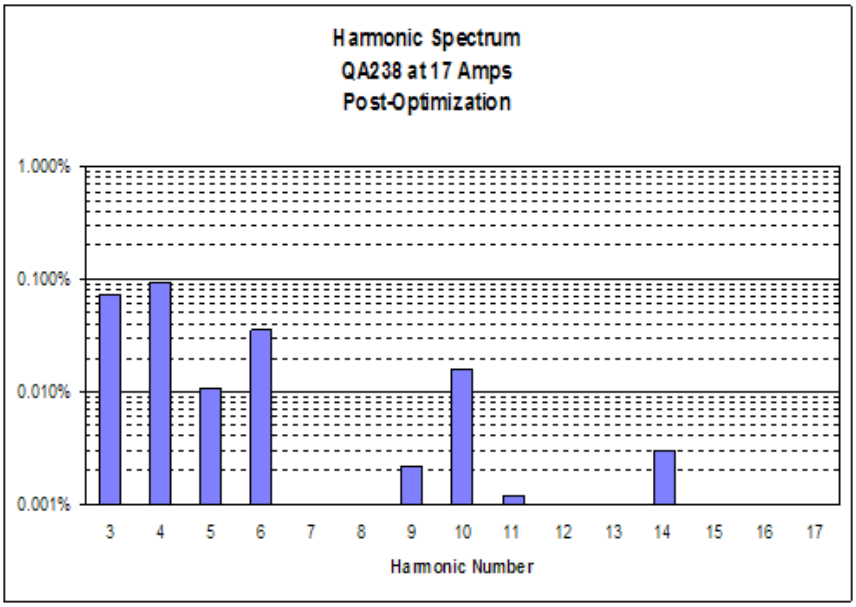

Figure 4: Quad QA238 measured at 17 amps

Recently, quad QA238 was remeasured at 17 Amps after significant improvements were made in the magnet measurement test stand [8]. Figure 4 shows the magnitude of the multipole terms. As seen from that, they all are within or

below 1E-3. This is several times under our proposed specification.

5 Dipole magnet modelization results

TOSCA was used to estimate the field integrated along the magnet trajectory [4],[5]. Individual multipole components were evaluated by Fourier analysis on a circle and gave B_1xL,B_2x^2L, $\ldots B_nx^nL$. The field expansion can be written as (8):

$$B_y(x)L \;=\; B_0\rho\left(\frac{L}{\rho}+\frac{B_1xL}{B_0\rho}+\frac{B_2x^2L}{B_0\rho}+\ldots+\frac{B_nx^nL}{B_0\rho}\right) \tag{8}$$

Equation (8) can be used to express the relative field error at a distance x in terms of multipole components K_n:

$$\frac{\Delta B_y(x)L}{B_0L} \;=\; \rho\left(K_1x+\frac{K_2x^2}{2}+\ldots+\frac{K_nx^n}{n!}\right) \tag{9}$$

On a per-multipole basis, the relationship between relative field error at a specific distance x_0, and the corresponding multipole is:

$$\left(\frac{\Delta B}{B}\right)_{n,x_0} \;=\; \rho\frac{K_nx_0^n}{n!} \tag{10}$$

Using (11), the values for the K_n^{EL} for ELEGANT were obtained. This was done at a radius $x_0 = 1\ cm$ where the field error had been evaluated from the TOSCA model. The equivalent DIMAD multipoles were obtained using eq.12.

$$K_n^{EL} \;=\; n!\left(\frac{\Delta B}{B}\right)_{n,x_0}\frac{1}{x_0^n}\frac{1}{\rho} \tag{11}$$

$$K_n^{DM}L \;=\; K_n^{EL}L\frac{1}{n!} \tag{12}$$

Models for all magnet types were made and multipoles were evaluated. This accounts for the systematics in the dipoles representing effects arising from the shape of the poles and the steel staturation.

Random errors generated by mechanical imperfections during the machining and assembly were estimated elsewhere [11].

5.1 Arc Dipoles

In order to set an error budget to take into account construction errors and misaligments, particle tracking was used in this work as well as in [1]. Previous work done on ArcA [1] is essentially in agreement with this work. Table 5 summarizes results from [1]. The octupole component was not taken into account in this earlier work.

	MBE1m(16) ARC1	MBR2m ARC2	MBE1m ARC3	MBB2m ARC4,5,6	MBA3m ARC7,8,9	MXP4m ARCA
K_2L (m^{-2})	0.35	0.22	0.24	0.12	0.11	0.07
K_3L (m^{-3})	2.22	3.51	8.31	4.21	2.20	2.26
K_4L (m^{-4})	543	1390	327	166	215	148
$\frac{B^{'}L}{BL}$ (m^{-1})	0.022	0.020	0.036	0.018	0.015	0.010

Table 4: Expected DIMAD multipole values from TOSCA calculations (no construction errors)

	MXP4m ARCA
K_2L (m^{-2})	0.15
K_3L (m^{-3})	0.0
K_4L (m^{-4})	236.0
$\frac{B^{'}L}{BL}$ (m^{-1})	0.078

Table 5: DIMAD multipole specification obtained from [1]

Generalizing to the other arcs was done by taking the multipole components from table 4 and scaling them by a factor of six. This is a simple way to add room for the random construction errors and has been used elsewhere [6].

TOSCA gives a relatively accurate estimate of what saturation effects will be and these will depend on the design of the magnet and the field at which they are run.

In the case of the second step dipoles in the spreader/recombiner/transport recombiners, these effects are significantly bigger than in the arcs. We set the specification there by adding roughly the same amount of construction error room as given by the arc dipoles of the corresponding passes rather than just scale by a factor of six the field errors which would have resulted in unphysically big field errors specifications for the second step dipoles.

Following this approach, we arrived at the final multipoles specifications, for each ARC dipole, given in table 6.

	MBE1m(16) ARC1	MBR2m ARC2	MBE1m ARC3	MBB2m ARC4,5,6	MBA3m ARC7,8,9	MXP4m ARCA
K_2L (m^{-2})	1.74	1.08	1.19	0.60	0.54	0.33
K_3L (m^{-3})	11.1	17.54	41.56	21.07	11.01	11.28
K_4L (m^{-4})	2714	6951	1636	829	1071	740
$\frac{B^{'}L}{BL}$ (m^{-1})	0.11	0.10	0.18	0.09	0.08	0.05

Table 6: Proposed specifications for DIMAD K_nL

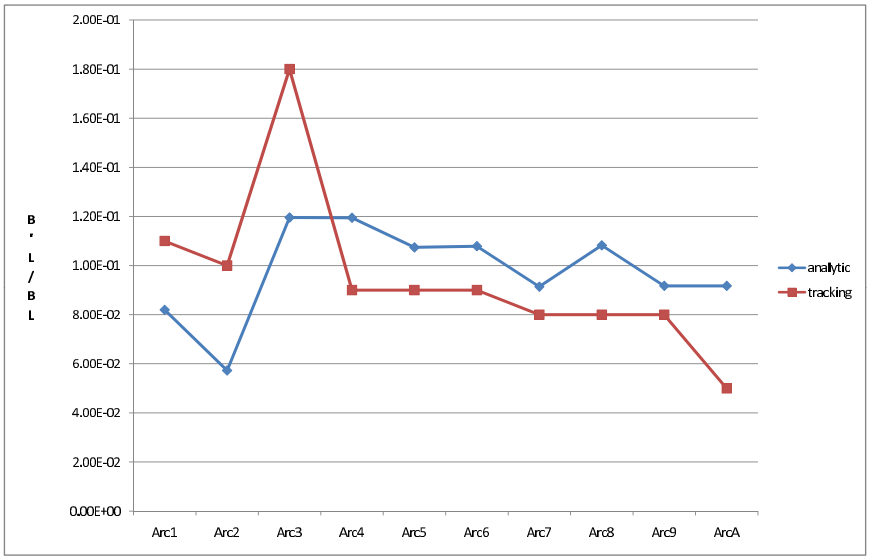

Figure 5: comparison between analytical specs and tracked specs for $\frac{B^{'}L}{BL}$ (m^{-1})

The $\frac{B^{'}L}{BL}$ is computed for the non linear terms and does not include the quadrupole term as it is linear and readily correctable by adjusting quadrupoles in the lattice.

5.2 comparison with the analytical approach

In TN-06-030, an analytical approach was chosen to estimate the field error tolerances in the arc dipoles. The criterion was that the effect of all the non-linearities should not result in more than 10 % of mismatch. Dipoles were allowed to have a sextupole and decapole component. No octupole was taken into account.

Given this, table 7 gives the multipole values (in the DIMAD convention) derived from the analytical approach. Figure 5 shows the analytical specification versus the tracked specification in terms of $\frac{B^{'}L}{BL}$ computed at 1cm.

	MBE1m(16) ARC1	MBR2m ARC2	MBE1m ARC3	MBB2m ARC4,5,6	MBA3m ARC7,8,9	MXP4m ARCA
K_2L (m^{-2})	1.59	1.11	1.16	1.16	0.89	0.89
K_4L (m^{-4})	194	136	142	142	109	109
$\frac{B^{'}L}{BL}$ (m^{-1})	0.082	0.057	0.12	0.12	0.11	0.092

Table 7: K_nL Specifications arrived at via the analytical approach

5.3 Spreader, recombiner and transport recombiner dipoles

The spreader, recombiner and transport recombiner dipoles were modeled in TOSCA and multipoles were obtained. The trapezoidal dipoles (second BCOM) as well as the first BCOM (rectangular) were modeled on a per-pass basis.

All other second pass magnets (MAI's and such) were considered together. Their sagitta being similar, the field errors were computed along one single reference trajectory. Multipoles were then obtained using (11) for the ELEGANT multipoles and and (12) to compute the equivalent DIMAD multipoles.

Following the same approach, we multiplied the TOSCA values by five to budget for random construction and assembly errors.

Magnet	K2L (m^{-2})	K3L (m^{-3})	K4L (m^{-4})	$\frac{B'L}{BL}$
MAI1S04,S06,R01,R03	4.09	32.61	5931.53	0.15
MAI1S03,R04	4.05	32.24	5865.72	0.15
MAI2S04,2S06	1.51	21.95	6579.16	0.14
MAI3S04,3S06,3R01,3R03	1.48	43.71	1965.89	0.22
MAV3R04,3S03	1.74	51.43	2313.18	0.15
MAL2S03,2R04	1.15	16.67	4996.89	019
MAA3S04,3S06	1.48	43.71	1965.89	0.28
MAV4S03,4R04	0.73	19.32	956.79	0.14
MAF4S04,4S06,4R01,4R03	0.82	21.45	1062.38	0.14
MAC5S04,5S06,5R01,5R03	0.47	12.4	614.29	0.14
MAU5S03,5R04	0.66	17.24	853.85	0.14
MAU6S03,6R04	0.46	12.19	603.83	0.14
MAB6S04,6S06,6R01,6R03	0.61	16.03	793.95	0.14
MAC7S04,8S06,7R01,7R03	0.25	4.25	416.43	0.14
MAE8S04,8S06,8R01,8R03	0.38	6.54	641.1	0.14
MAR9S06,9R01	0.27	4.62	452.46	0.14
MXHAS05,AR01,MAHAS06	0.25	5.64	423.09	0.10
MARBS07,BS08	0.18	4.14	310.56	0.10

Table 8:Proposed specifications for second step dipoles

Table 9: Proposed specifications for Common Dipoles

Magnet	K2L (m^{-2})	K3L (m^{-3})	K4L (m^{-4})	$\frac{B'L}{BL}$
MAQ1S01,1R06	1.1	13.5	8233	0.06
MAQ3S01,3R06	0.39	4.8	2943	0.06
MAQ5S01,5R06	0.24	2.94	1792	0.06
MAQ7S01,7R06	0.17	2.11	1288	0.06
MAQ9S01,9R06	0.13	16.48	1005	0.06
MAQBS01,BR06	0.11	1.35	824	0.06
MAS3S02,3R05	0.75	27.0	221	0.1

Table 9: *continued*

Magnet	K2L (m^{-2})	K3L (m^{-3})	K4L (m^{-4})	$\frac{B'L}{BL}$
MAS5S02,5R05	0.46	16.44	135	0.1
MAS7S02,7R05	0.33	11.81	97	0.1
MAS9S02,9R05	0.12	1.52	928	0.06
MASBS02,BR05	0.10	1.25	761	0.06
MAW2S01,2R06	0.65	7.94	4843	0.06
MAW4S01,4R06	0.33	4.08	2488	0.06
MAW6S01,6R06	0.22	2.75	1674	0.06
MAW8S01,8R06	0.17	2.07	1261	0.06
MAWAS01,AR06	0.14	1.66	1012	0.06
MAX4S02,4R05	0.57	20.29	166	0.1
MAX6S02,6R05	0.38	13.65	112	0.1
MAX8S02,8R05	0.29	10.28	84	0.1
MAXAS02,AR05	0.11	1.36	83	0.06

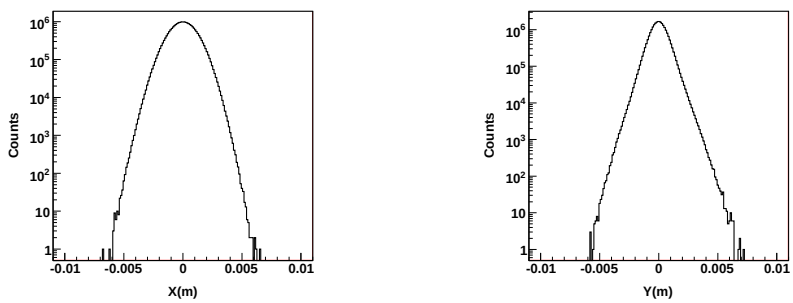

Figure 6: Horizontal and Vertical beam profiles at radiator in hall D for the specification

This was validated by full particle tracking on the parallel computing facility. Forty millions particles were tracked from the exit of the injector to the entrance of hallD. This resulted in mismatches and emittance growth within tolerances.

Figures 8 and 7 show the outcome of the transverse x and y distributions at the hallD radiator.

Multipole effects are clearly visible. They are somewhat washed out in the horizontal plane because of the synchrotron radiation.

Keeping in mind that these effects are suppressed by several orders of magnitude, the specifications proposed in table 6 are adequate and they have a safety margin of another factor of two provided one keeps the sextupole term under control.

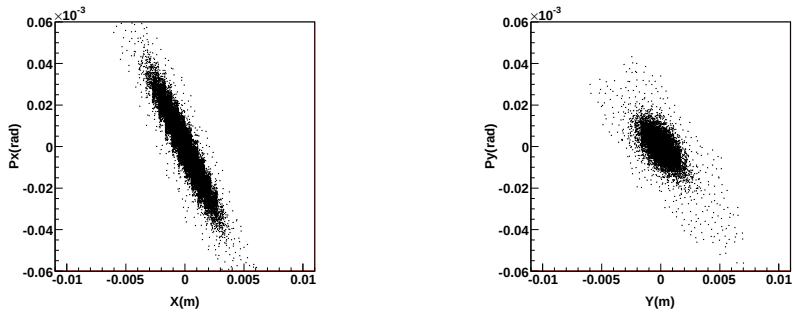

Figure 7: Horizontal and Vertical phase-space at radiator in hall D for the specification

5.4 septa magnets

In the beam switchyard area of the machine, the fifth pass can have up to three parallel beams vertically separated for each hall. Hall A is the one on top, hall B in the middle and hall C in the bottom. The separation is about 1cm between beams at the start of the BSY area. These three parallel beams are then deflected horizontaly via a lambertson magnet and a pair of septa magnets (MYRAT03 and MYR8T04). The resulting three beams are send on their way to their respective halls via second order achromatic transport channels. One area of concern is the required field quality (in terms of multipoles) in these two septum magnets. The A beam is the closest to the top edge. Multipole content was computed in these magnets for various trajectories taken nearly parralel to the magnet edge along the whole magnet. We then gradually scaled up this multipole distribution until the phase-space distortion and halo became borderline.

table 10 gives the upper limit on the values for the multipoles and the resulting $\frac{B^{'}L}{BL}$ for an A beam located 2cm away from the edge of the magnet along the whole length.

Table 10: A beam located 2cm away from top edge of MYR in 5th pass

Magnet	K2L (m^{-2})	K3L (m^{-3})	K4L (m^{-4})	$\frac{B^{'}L}{BL}$
MYRAT03,8T04	3.0	81.5	2854	0.14

The resulting distortions are equivalent to about three times what the ArcA specification was set to be.

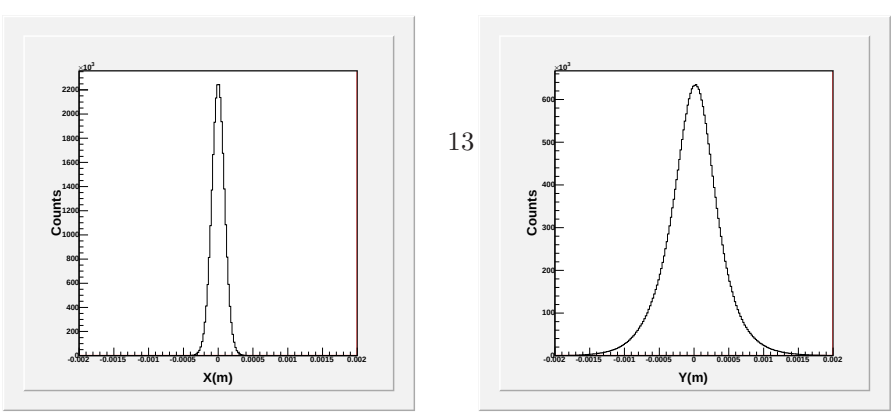

Figure 8: Horizontal and Vertical beam profiles at Compton for Hall A beam

In practice, the situation we evaluated is a worst case scenario. It is possible

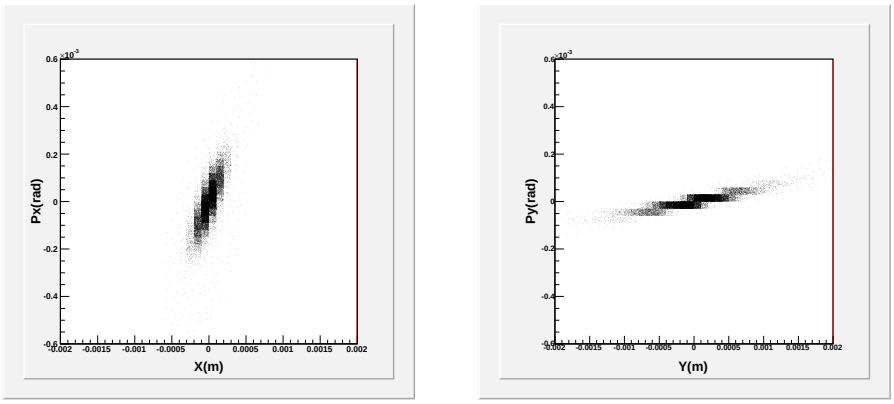

Figure 9: Horizontal and Vertical phase-space at Compton for Hall A beam

6 Effect of skew multipoles

6.1 Skew quadrupole term

We estimated the effect of a skew quadrupole component on the dipole magnets. Studies were done with systematic skew components. Separate studies show that the amount of skew quadrupole arising from end effects and steel saturation are negligeable. The bulk of the skew errors will come from manufacturing errors at the poles. We chose to simulate the worst case scenario for which all the skew components are the same at each magnet rather than randomly distributed. This could happen if the error arise from the manufacturing process rather than assembly.

The effect of the skew component on the beam is twofolds. First, the transport becomes coupled. Secondly, emittance leaks from the horizontal to the vertical plane. We assessed the amount of coupling by exciting the lattice with an orbit of about 1mm in amplitude in the horizontal plane. The resulting vertical orbit was then read off for various distributions of skew quadrupoles. Figure 10 shows the situation where one has a skew component of $J_2L = 10^{-3}m^-1$ distributed systematically on all 32 dipoles. This corresponds to about 1 Gauss/cm. The resulting vertical orbit is measurable by the bpm system, growing to about 100μ in amplitude by the end of the Arc.

The resulting mismatch is mainly in the vertical plane (about 10 % versus 3% in the horizontal plane).

The coupling of the X and Y plane will have an effect on the performance of the steering systems. One can estimate the impact on the degradation of the 2D steering.

A normal multipole component produces kicks in the transverse planes as given in eqs (13) and (14).

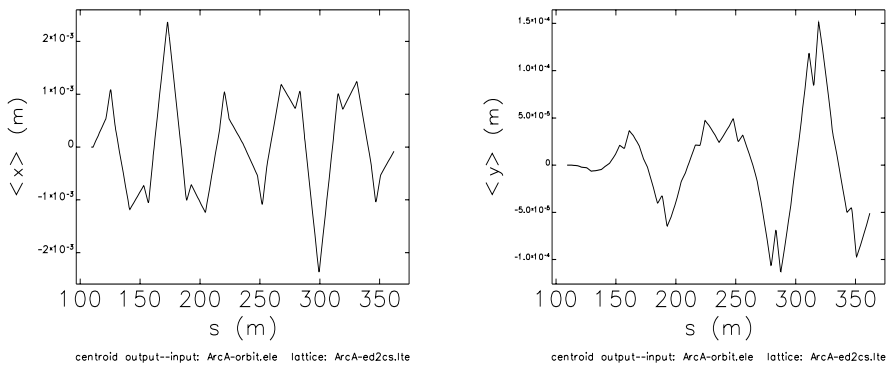

Figure 10: Left is horizontal orbit, right is resulting coupled vertical orbit for a skew quadrupole component $J_2 L = 10^{-3} m^{-1}$.

$$\Delta\theta_x = -\frac{B_n L}{B\rho}\frac{r^n}{n!}\cos(n\theta) \tag{13}$$

$$\Delta\theta_x = \frac{B_n L}{B\rho}\frac{r^n}{n!}\sin(n\theta) \tag{14}$$

$$r = \sqrt{x^2 + y^2} \tag{15}$$

For a skew component, one must rotate the reference frame by the amount of skew, evaluate the kicks in the rotated frame and rotate back in the lab frame.

Given that

$$V^{\vec{lab}} = \left[x, x^{'}, y, y^{'}, l, \delta\right]^T \tag{16}$$

$$R_\alpha = \begin{bmatrix} \cos\alpha & 0 & \sin\alpha & 0 & 0 & 0 \\ 0 & \cos\alpha & 0 & \sin\alpha & 0 & 0 \\ -\sin\alpha & 0 & \cos\alpha & 0 & 0 & 0 \\ 0 & -\sin\alpha & 0 & \cos\alpha & 0 & 0 \\ 0 & 0 & 0 & 0 & 1 & 0 \\ 0 & 0 & 0 & 0 & 0 & 1 \end{bmatrix} \tag{17}$$

$$\Delta\vec{V^s} = R_\alpha . V^{\vec{lab}} \tag{18}$$

$$\tan\theta = \frac{\Delta\vec{V^s_y}}{\Delta\vec{V^s_x}} \tag{19}$$

$$\vec{V^s} = \Delta\vec{V^s} + \left[0, -\frac{B_1 L}{B\rho}\frac{r^n}{n!}\cos n\theta, 0, \frac{B_1 L}{B\rho}\frac{r^n}{n!}\sin n\theta, 0, 0\right]^T \tag{20}$$

$$V^{\vec{slab}} = R_{-\alpha} . \vec{V^s} \tag{21}$$

If we enter in the midplane ($y = 0$) with zero angle, the resulting kicks from skew components can be expressed at any multipole order as :

$$\Delta\theta_x = 0.0 \tag{22}$$

$$\Delta\theta_y = -\frac{B^{'} L}{B\rho}\frac{x^n}{n!} \tag{23}$$

while the kicks from the normal components are given by

$$\Delta\theta_x = -\frac{B^{'} L}{B\rho}\frac{x^n}{n!} \tag{24}$$

$$\Delta\theta_y = 0.0 \tag{25}$$

For n=1, we recover the quadrupole results, n=2 gives the sextupole term and n=4 the decapole term.

To get an idea of the scale of this effect, we can equate that to a roll error in a dipole which would read:

$$\Delta\theta_x = \frac{B\cos\theta_r L}{B\rho} \tag{26}$$

$$\Delta\theta_y = -\frac{B\sin\theta_r L}{B\rho} \tag{27}$$

Comparing the two, we get the equivalent roll angle θ_r to be

$$B_m = G_m \frac{x^m}{m!} \tag{28}$$

$$\sin\theta_r = \frac{B_m L}{BL} \tag{29}$$

Table 11 gives the kick and equivalent roll for the skew quadrupole, sextupole and decapole kicks, for a gradient $G_m = 1.0\ Gauss/cm^m$ and a beam off-centered by $x = 0.1\ cm$.

Order	kick(rad)	roll (rad)
1	1.09e-6	11.1e-6
2	5.55e-7	
4	0.46e-7	

Table 11: multipole kicks for off-centered, on midplane, beam

Looking at table 11, one sees that only the skew quadrupole really matters. (also see section 6.2 for more discussion on that point)

As a reminder, the 12GeV error budget allocates 1.0 $mrad$ to the dipole roll. If the dipole are installed with significantly less roll, then one could absorb the coupling error in this error budget and set the limit to 1 Gauss/cm.

Another way to picture the effect is to imagine a vertical corrector located at the middle of each dipole and kicking the beam by $1.0\mu rad$. We carried out the estimate numerically using Elegant, asking it to resteer the vertical orbit to compensate for the effect of the skew kicks.

Otherwise, one can add this equivalent roll error to the original error budget and get an estimate of the effect of skew quadrupoles on the steering.

We would like to keep the coupling below the level that one has to correct for it, hence one can set the limit to be $J_2L < 5.010^{-4}m^{-1}$ (less than 0.2 G/cm) which brings it down to below the bpm accuracy of 20μ.

This specification could be relaxed if one designs a 4D steering algorithm to maintain the beam at the required stability.

6.2 higher order skew terms

For the higher order skews, the situation is slightly different. Both normal and skew components will give coupling. Hence, the skew terms become relatively indistinguishable. This is more and more true as the order of the multipole increases (the angle diminishes). The main effect these skew terms have is emittance growth.

There is no need to set a separate specification for the skew components. It is sufficient that the combined amplitude (quadradic sum) of the skew and normal component stays below the $\frac{B'L}{BL}$ specifications we already gave.

Figure 11 shows the vertical and horizontal mismatch distribution in percent, for two hundreds random multipoles distributions for which the amplitude $a = \sqrt{K_{2r}^2 + J_{2r}^2}$ was kept constant but the mix between normal and skew component was varied. As seen from these histograms, there is no need to distinguish between emittance growth coming from the normal or skew components.

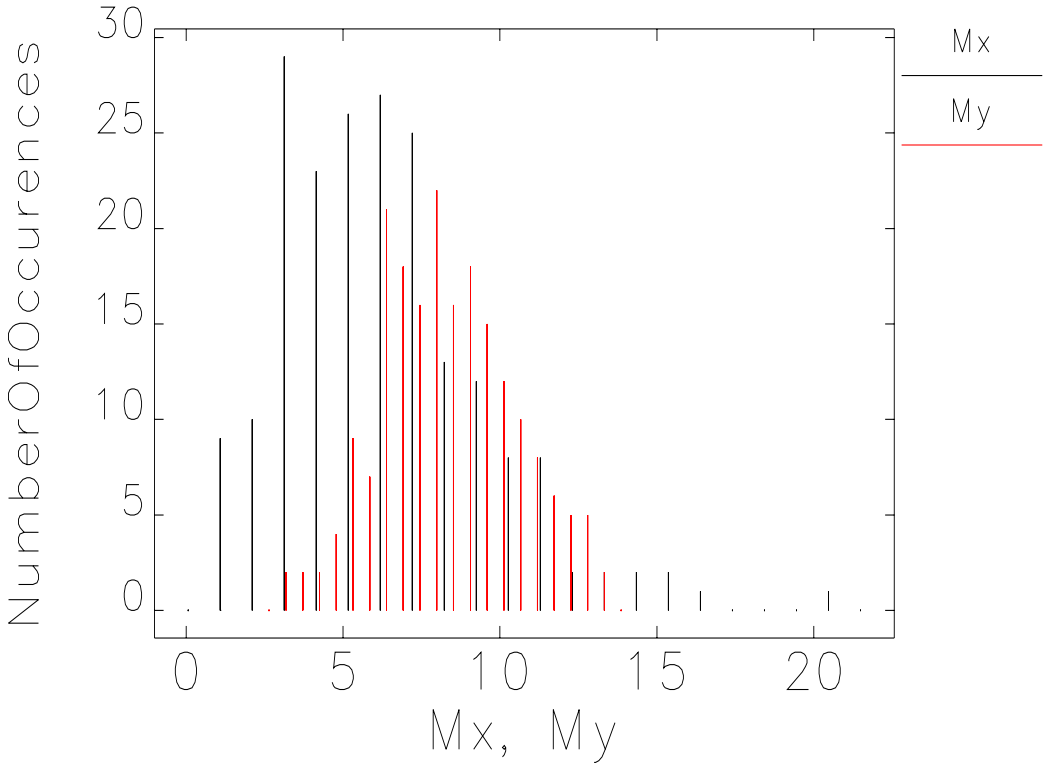

Figure 11: decapole mismatch in percent for various combinations of normal and skew with total amplitude kept constant

References

[1] Pozdeyev, E. *An estimate of the maximum acceptable strength of field inhomogeneities in Arc 10 dipoles and quadrupoles of the 12 GeV CEBAF upgrade*, TJNAF technical note JLAB-TN-06-029

[2] Borland, M.*Elegant: A flexible SDDS-compliant code for accelerator simulation.*, LS-287 ANL technical report, Argonne National Lab, 2000.

[3] M. Tiefenback, J. Bengtsson, *private communication.*

[4] Benesch, J.*The 3m arc dipole(BA)- modeling and comparison with sparse experimental data*, TJNAF technical note, JLAB-TN-08-022

[5] Benesch, J. *Calculating multipoles in OPERA/TOSCA - mesh and software noise effects* ,TJNAF technical note JLAB-TN-08-024

[6] SLAC-R-609, SPEAR 3 design report

[7] Benesch, J. *QA quadrupole field quality*, TJNAF technical note JLAB-TN-07-006

[8] Bagget K., Beck M., Hiatt T., Sullivan K. *MetroLab PDI Measurement System Performance Optimization.* ,TJNAF technical note JLAB-TN-06-018

[9] Halback K., *First Order Perturbation Effects in Iron-Dominated Two-Dimensional Symmetrical Multipoles*,NIM-74-1, 1969, 147-164

[10] *Dipole Field Inhomogeneities and the "Yunn Effect"* D. Douglas, B. Yunn, JLAB-TN-97-019

[11] *Determination of the influence of machining defects on magnetic fields.* N. Ruiz, JLAB-TN-08-060